Development of a model for detection of saline blanks amongst mangrove species on hyperspectral image data

Somdatta Chakravortty* and Dipanwita Ghosh

Department of Information Technology,
Government College of Engineering and Ceramic Technology,
Kolkata 700 010, India

In this study we apply hyperspectral imagery to identify saline blank patterns within the mixed mangrove forest of Sunderban Bio-geographic Province, West Bengal, India. We use derivative analysis to identify hyperspectral wavelengths that are sensitive to the presence of minerals comprising saline blanks. These wavelengths have been considered for development of a novel saline blank identification model. The wavelength showing derivative value with maximum absorption in the SWIR region at 1780 nm and maximum reflection in the red region at 690 nm has been extracted for development of saline blank index. This index has been compared with the existing salinity indices and a detailed analysis has been carried out. It is found that the index outperforms existing salinity indices – normalized differential salinity index and salinity index, and accurately detects the saline blank areas of Henry Island of the Sunderbans Delta. The accuracy of pixels identified as saline blank pixels has been assessed by comparing the overall accuracy with other existing indices. Physical sampling has also been carried out and the salinity results have been compared with the image-derived results.

Keywords: Saline blanks, hyperspectral data, mangroves, derivative analysis.

THE Sunderban mangrove ecosystem is the largest single-patch mangrove forest in the world that offers a closed, continuous and unique ecological niche of varied mangrove species[1]. Yet the Sunderban mangroves represent one of the most threatened and vulnerable ecosystems that have experienced a traumatic decline in areal extent and species diversity over the last few decades[2]. This has necessitated detailed species-level classification and mapping of mangroves that would help identify the extent of damage to this floral community[3]. Saline blanks are common features of the mangrove ecosystem that exists in an active deltaic environment[4]. Saline blanks, prior to their formation, are initially lowlands that have the capacity to store water for longer time during high tide. The accumulated water later gets evaporated, leaving the salt and sediments behind. With gradual rise in salinity, these saline-rich areas become inadaptable and gradually become devoid of mangrove cover. The presence of saline blanks exerts a mixed influence on the distribution of mangrove species. Saline blanks are good for the growth of *Ceriops decandra* and *Excoecaria agallocha*, while they are detrimental to Sundari (*Heritierra fomes*), Dhundul (*Xylocarpus granatum*) and Possur (*Xylocarpus mecongensis*). In Bangladesh, due to increase in saline blanks, about 40% of mangrove cover is affected by tip-dying disease. Presence of saline blanks is good for *Avicennia marina* and *Avicennia alba*, which have excellent stilt root system and high pneumatophore density and prefer a more saline environment for their survival.

Remote sensing is a convenient tool for pattern recognition and change detection of mangrove forests and saline blanks that exist within them over space and time[5,6]. Few studies have been done in India on species-level classification of mangroves with the use of hyperspectral data. Further, change detection studies on the nature and distribution of saline blanks and pattern recognition of the economically important mangrove species that surrounds these vital eco-significant spots for restoration/rehabilitation purpose and economic use are rarely reported at the national and international level[7,8]. The main objective of this study therefore is, to develop a model for saline blank detection using image processing of hyperspectral data[9]. Interestingly, the use of hyperspectral image classification algorithm for discrimination of saline blanks is a unique attempt in India and is a hitherto unexplored field of research for Indian mangroves in general.

It is observed that the soils forming saline blanks are present in encrustations; hence the reflectance of soil surface is very high in the visible and NIR region of the electromagnetic spectrum[10]. It is also observed that characteristics of soil surface such as colour and type are good indicators to identify soil salinity[11,12]. Studies suggest that salts present in saline blanks are mostly halite, hydrated chloride, sulphate, suphide and some organic matter[13]. In these soils, halites such as hydrated sodium chloride (NaCl) are present in the form of (Na^+) and (Cl^-) ions. The sodium ion (Na^+) is the most important component that makes the soil saline in nature. Seasides have sulphates such as magnesium sulphate ($MgSO_4$) and calcium sulphate ($CaSO_4$) that are present in the form of calcium (Ca^{2+}) and magnesium (Mg^{2+}) ions which make the soil more saline. As the calcium and magnesium ions have higher clay-binding capability, the saline soils become clayey or hydrated in nature that makes them harmful for plant growth. Conventional methods of soil sample analysis have been practised till date to detect salinity of soils. In recent times, hyperspectral remote sensing has proved to be a useful tool to predict soil salinity[13–15]. Using this technology, it is possible to analyse spectral information of highly saline soils in detail. Recent studies have used multispectral sensors such as Landsat Thematic Mapper (TM), Landsat Multispectral Scanner System (MSS), Landsat Enhanced Thematic Mapper Plus (ETM+), SPOT, Advanced Space borne

*For correspondence. (e-mail: csomdatta@rediffmail.com)

Thermal Emission and Reflection Radiometer (Terra-ASTER), Linear Imaging Self-scanning Sensor (LISS-III) and IKONOS to analyses soil salinity in saline blanks[16,17]. However, owing to the lack of spectral details, multispectral sensors do not give accurate detection results.

The main objective of this study is to use hyperspectral data to develop an algorithm for automatic detection of saline blanks that exist within pure and mixed patches of mangrove cover.

As a case study, we have selected the pristine mangrove habitats of the Sunderban Biosphere Reserve, West Bengal, India. The study will focus the Henry Island (Figure 1) which is around 10 sq. km. in area, extends between 88°12′–88°26′E long and 21°35′–21°40′N lat and covers topographic sheet no. 79C/2 (Figure 1). The selection of the study area is based on the fact that the Island provides an ideal locale for saline blanks surrounded by dwindling mangrove species, majority of which are ecologically rare, endangered and endemic.

We have used hyperspectral data acquired on 27 May 2011 by the hyperion sensor on-board the Earth Observatory-1 (EO-1) satellite. The hyperspectral image has a spatial resolution of 30 m and a wide spectral range from 355 to 2577 nm, with a narrow bandwidth of 10 nm.

Fast Line-of-Sight Atmospheric Analysis of Spectral Hypercubes (FLAASH) model in ENVI software has been used for atmospheric correction to convert the radiance values in the image to its reflectance values. FLAASH is an atmospheric correction tool that has to be added separately to ENVI software and corrects wavelengths in the visible through near-infrared and shortwave infrared regions, up to 3 μm. Unlike many other atmospheric correction programs that interpolate radiation transfer properties from a pre-calculated database of modelling results, FLAASH incorporates the MODTRAN4 radiation transfer code. Water vapour and aerosol retrieval are only possible when the image contains bands in appropriate wavelength positions.

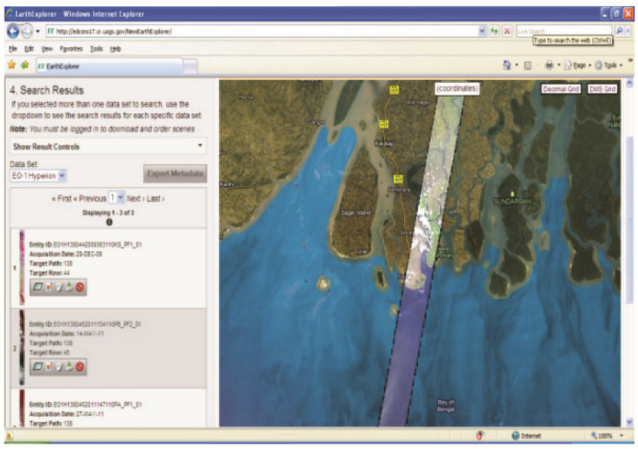

Figure 1. Location of the study area.

Ground survey of the study area was conducted to identify and collect samples of saline blanks whose image-based classification has been carried out. Global positioning system (GPS) has been used to precisely locate the geographical coordinates of the study area. As most of the saline blank areas exceed 900 sq. m (the spatial resolution of hyperion pixels), sampling was done in open saline blank areas and no subpixel level measurements were made. The total area covered by saline blank patches under study is 0.258 sq. km.

The area occupied by saline soil was measured and the ground survey areas were used as reference points for accuracy assessment of image-derived findings. Figure 2 displays the spectral profile of a saline blank pixel plotted at 21°34′23.44″ lat and 88°17′50.97″ long. Soil samples were collected from the saline blank areas and analysed. They showed high to very high salinity values (Table 1). The application of saline blank index on the hyperspectral image of the study area also identified those pixels that represent saline blanks. The literature on Sunderban saline soils (estuarine conditions) indicates the presence of minerals such as halite (sodium chloride), sulphate (calcium sulphate) or gypsum, magnesium sulphate and other sulphides[18].

Derivative analysis has shown potential in spectral analysis of remotely sensed data. Derivative spectra give emphasis to small details in the spectra and minimize atmospheric effects in the image data. They are appropriate for extracting spectral features related to specific characteristics of target objects – saline blank soils in this case. In case of first derivatives, if reflectance values of

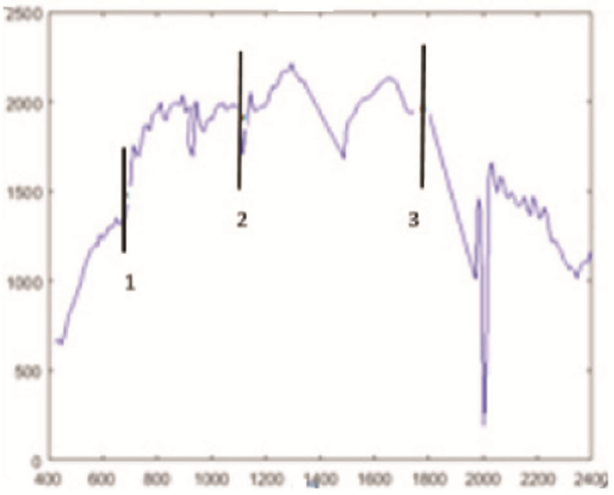

1	690 nm wavelength
2	1104 nm wavelength
3	1780 nm wavelength

Figure 2. Spectral profile of saline blank pixel with wavelengths of interest.

two adjoining bands do not vary much, then the information in each band can be characterized with only one band. The second derivative identifies bands that may be represented by a linear combination of contiguous bands. The higher the derivative value, indicating higher deviation, more is the information on the band. The second derivative and derivatives of higher order are more insensitive to variations in illumination. Though researchers have used higher order derivatives in several studies, second-order derivatives are more common. This study thus uses second derivative values for identifying the presence of minerals in saline soils by determining absorption band positions specific to the minerals. The derivatives show a negative value at absorption band positions when they are calculated for the reflectance values of the spectra. Though first derivative values have been calculated and displayed, they have not been used for data analysis in this study. The derivatives have been estimated using suitable difference schemes and a fixed wavelength interval Δw, between successive hyperspectral bands. The first derivative has been estimated as

$$\mathrm{d}x/\mathrm{d}w = [x(w_i) - x(w_{i-1})]/\Delta w, \quad (1)$$

where Δw is the wavelength interval between bands, and $x(w_i)$ is reflectance at the ith band whose derivative is being evaluated.

The second derivative used for analysis is derived from the first derivative as

$$\mathrm{d}^2x/\mathrm{d}w^2 = [x(w_i) - 2x(w_{i-1}) + x(w_{i+1})]/\Delta w^2. \quad (2)$$

The derivative values have been used to determine the band positions having peak reflectance values, low absorption values in the reference spectra of saline blanks. These wavelength bands are sensitive to the presence of specific minerals and signify their presence in the saline soil.

Formation of saline blanks is a deterrent for the growth of mangrove community and thus it is necessary to properly identify and delineate them for management of the mangrove ecosystem. There are several salinity indices existing in the literature such as Normalized Differential Salinity Index (NDSI), Salinity Index (SI), etc. that have been used for identifying saline soil pixels from remotely sensed hyperspectral data. However, it is not possible to identify and classify different types of saline soils in an area using these indices. Though identification of saline blank has been done through physical survey, it has not been attempted through interpretation of remotely sensed data. As saline blanks exist within dense mangrove forests, it becomes extremely difficult to conduct extensive field studies for physical sampling. Thus, it was felt necessary to develop an index that can be exclusively used for saline blank detection. As the prime objective in this study is to identify saline blank areas of Henry Island, the bands that are sensitive to the presence of minerals comprising saline blanks have been identified. The spectral profile of saline blank extracted from ground survey has been considered as the reference spectra. The second derivative has been calculated from the saline blank soil spectra and been analysed to identify the saline soil-sensitive bands. It has been observed that beach and agricultural soils have brighter pixel values, while others have lower values due to the presence of clay and water. Thus, the brightness index has been initially applied on the image, and pixels with index values of 0.5 and above have been removed. This eliminates the beach and agricultural soils from the study area. The following brightness index has been applied

$$\text{Brightness index} = \sqrt{\frac{(B_{1780})^2 + (B_{1104})^2}{\text{Maximum} \times \text{brighness value}}}. \quad (3)$$

This index is then applied on the masked-out image where all pixels with index values above 0.1 have been identified as belonging to saline blank area. The saline blank detection index (SBDI) model developed here in its general form is as follows

$$\text{SBDI} = \frac{B_{\text{swir}} - B_{\text{red}}}{B_{\text{swir}} + B_{\text{red}}}. \quad (4)$$

After application of selected bands, new index is

$$\text{SBDI} = \frac{B_{1780} - B_{690}}{B_{1780} + B_{690}}. \quad (5)$$

The basis of selection of the above wavelength bands from second-derivative results has been mentioned in detail below.

As the prime objective is to identify saline blank areas of Henry Island, the bands that are sensitive to the presence of minerals comprising saline blanks have been identified. The spectral profile of saline blanks extracted from ground survey is considered as reference spectra. The absorption and reflectance characteristics in the spectral profile of saline blanks (Figure 2) indicate the presence of minerals present in saline blank soils[15]. It is observed that there is high reflectance at 800 nm wavelength; hydrate absorption feature at wavelengths 980 and 1150 nm and water absorption feature at wavelengths 1450 and 1950 nm (ref. 13). These characteristics indicate the presence of sodium chloride, sulphate and sulphide. The spectra also shows a hydroxyl absorption feature at wavelength 2200 nm, water absorption feature at wavelengths 1450 and 1950 nm that indicates the presence of gypsum as well as calcium sulphate[13]. According to the JPL spectra of gypsum ($CaSO_4$), there is absorption at wavelengths 1200, 1440, 1740 and 1940 nm that closely

Table 1. Average salinity results for sampling locations of soil types in Henry island

Month-wise observation	Mangrove forest	Saline blank	Agriculture	Pisciculture	Beach
May	22	24	12	17	29
July	18	19	8	13	25
November	19	22	9	14	26
February	18.5	17	8.4	13.3	25.6

Table 2. Identification of various minerals using derivative analysis

Wavelength	First-derivative	Second-derivative	Identification of minerals
0.6914	2.6496	1.7555	Presence of saline soil
0.7931	0.7827	0.2452	Presence of saline soil
0.8033	3.2352	–0.9637	
0.8135	–6.4015	0.5	
1.033	3.7021	–0.4053	Hydrate absorption feature
1.1042	–18.8769	6.478	Presence of saline soil
1.2051	5.5031	–0.2273	Presence of gypsum
1.2959	–4.5639	0.5081	Presence of saline soil
1.306	0.5175	–0.1688	
1.3161	–1.17	0.7992	
1.4875	13.2774	–1.1061	Water absorption
1.7801	10.9967	–9.0649	Hydrate absorption feature
1.7902	–79.6527	12.1396	Presence of saline soil
1.9718	41.7432	–5.044	Water absorption
2.0021	41.136	5.2419	Presence of clay
2.2139	5.5559	–0.8875	Hydroxyl absorption as well as clay absorption
2.224	–3.3192	–0.703	Hydroxyl absorption as well as clay absorption

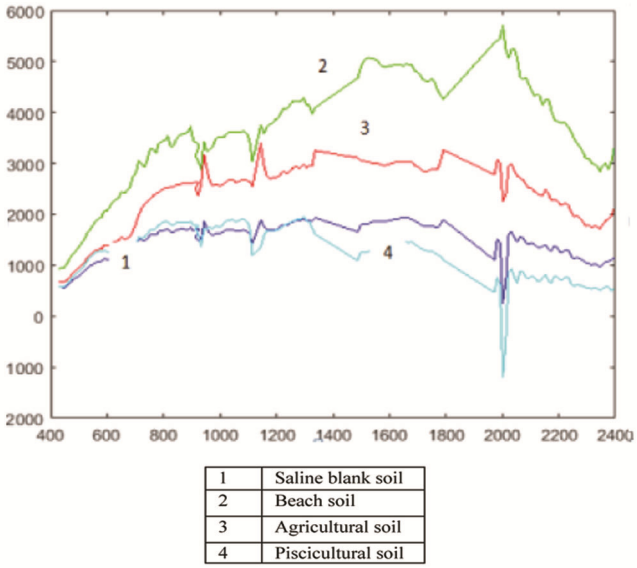

Figure 3. Spectral profile of saline soil pixels.

resembles the spectral features of saline soil spectra extracted from ground survey (Figure 2). This observation helps confirm the presence of gypsum in the extracted soil spectra. Deep absorption around the wavelength 2000 nm indicates the presence of clay, a physical property of the soil[13]. Reports of physical analysis of saline soil samples from this area also indicate the presence of these minerals. Due to estuarine conditions prevailing in the study area, the soil is mostly clayey in nature. Figure 3 displays the spectral profiles of saline soils extracted from pisciculture, agriculture and beach areas.

Salinity of soils is maximum in May, i.e. during the pre-monsoon period when the image was captured. Thus the saline pixels identified in the image have the highest salinity values of the year. Field samples have been collected and analysed for salinity during different seasons of the year that indicate that salinity values are lowest during July–September, i.e. the monsoon season, and gradually increase in November through April, with maximum in May and June (Table 1). Seventeen samples of saline blank soil, 10 samples of pisciculture soil, 10 samples of saline soil from agriculture area, 10 samples of soil from beach area and 10 samples from deep mangrove forest area have been collected during different seasons of the year and analysed for salinity. Table 1 shows the average values of each soil type.

This is a novel approach for automatic detection of saline blanks and is expected to specifically identify them from the hyperspectral image of the study area. Literature survey indicates that the features of minerals present in saline soils are best expressed in the shortwave infrared (SWIR) bands. The second-derivative values of saline blank spectra have been calculated (Table 2). In the SWIR region, at 1780 nm, the second-derivative results

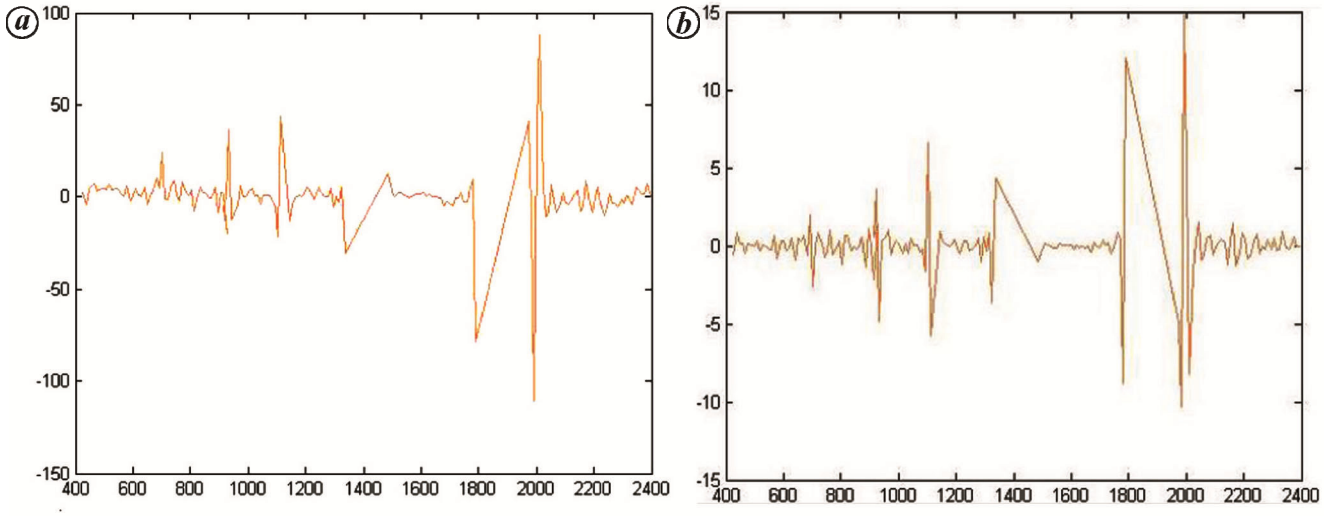

Figure 4. ***a***, First derivative of saline blank spectra at Δw = 10 nm. ***b***, Second derivative of saline blank spectra at Δw = 10 nm.

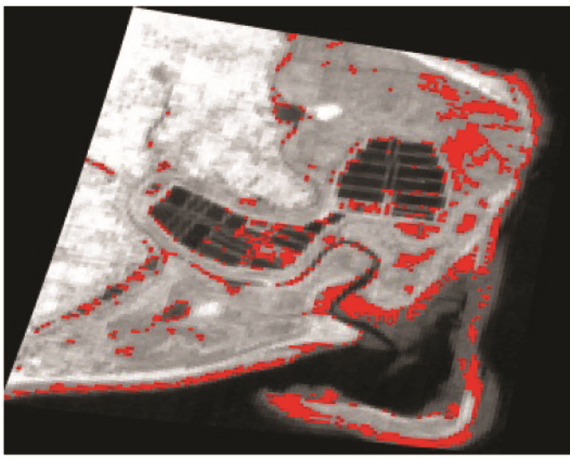

Figure 5. Soil retained (red pixels) after masking out brightness index values of 0.5 and above.

show the highest negative value indicating maximum absorption in the region (Table 2). This band also signifies hydroxyl-related absorption features that are indicative of salinity in the soil spectra. The spectral profiles of different saline soil end-members in the present study area also indicate variations in reflectance values in the red range of the bands. After derivative analysis of bands in the red region, it is observed that 690 nm wavelength shows the highest positive value, indicating maximum reflectance (Table 2). Thus this wavelength has also been selected for index development. Also, for index development we have considered the band with maximum absorption in the SWIR region and that with maximum reflectance in the red region. Figure 4 *a* and *b* displays the first- and second-derivative results of the hyperspectral band at an interval of 10 nm. In addition to the wavelength at 1780 nm, it is also observed that the derivative value at 1104 nm wavelength in the near infrared (NIR) region shows high reflectance and hence has been considered for calculation of brightness index. In Figure 2, the wavelengths at 1780 nm and 690 nm have been highlighted and marked. Figure 6 shows the results of application of brightness index on the image displaying those pixels (in red) that have been retained after masking out pixels with index values of 0.5 and above is shown in Figure 5. The SBDI is then applied on the masked-out image which identifies saline blank pixels as those with index values above 0.1 (Figure 6). Figure 2 shows the wavelengths considered for index development, while Figure 6 displays the saline blank areas (cyan) extracted after application of the proposed index.

There are some conventional salinity indices like NDSI and SI to measure soil salinity from hyperspectral image data. These indices are calculated considering the soil salinity-sensitive bands, i.e. the red and NIR bands of the hyperspectral data. The indices are calculated as follows

$$\text{NDSI} = (\text{Red} - \text{NIR})/(\text{Red} + \text{NIR}). \quad (6)$$

$$\text{SI} = \text{Red}/\text{NIR}. \quad (7)$$

Saline Blank Detection Index (SBDI) is similar to the NDSI, except that the NIR band has been replaced by SWIR band. This is because saline blank soils show more variation in the SWIR region and prominently display the salinity-sensitive absorption bands in this region. The red region also shows significant variations because of which it has been considered for index development.

The spectral profile of saline blank extracted from ground survey has been considered as the reference spectra (Figure 2). The mineral characteristic features have been compared with the standard spectral profiles of

Table 3. Index values at saline soil location of the study area

Land cover	Latitude	Longitude	NDSI	SI	BI	SBDI
Saline Blank	21°34′24.98″	88°17′53.13″	–0.2322	0.6262	0.4555	0.1761
	21°34′26.12″	88°17′52.36″	–0.2814	0.5610	0.4638	0.1924
	21°34′22.63″	88°17′52.06″	–0.2614	0.5892	0.4648	0.1855
	21°34′27.25″	88°17′53.84″	–0.2733	0.5702	0.4219	0.1575
	21°34′25.55″	88°17′52.26″	–0.2513	0.5992	0.4688	0.1744
	21°34′27.57″	88°17′53.76″	–0.2733	0.5702	0.4219	0.1575
	21°34′26.91″	88°17′55.14″	–0.3158	0.5164	0.4548	0.1936
	21°34′28.23″	88°17′53.16″	–0.3741	0.4501	0.4925	0.2083
	21°34′28.64″	88°17′53.16″	–0.3741	0.4501	0.4925	0.2083
	21°34′22.55″	88°17′51.89″	–0.2614	0.5892	0.4648	0.1855
	21°34′20.27″	88°17′42.13″	–0.3293	0.4960	0.4824	0.2117
	21°34′21.00″	88°17′42.40″	–0.2434	0.6050	0.4090	0.1645
	21°34′22.94″	88°17′43.37″	–0.3140	0.5155	0.4338	0.2466
	21°34′23.83″	88°17′43.90″	–0.2503	0.5975	0.4170	0.1792
	21°34′24.71″	88°17′35.22″	–0.4047	0.4101	0.4851	0.2082
	21°34′25.35″	88°17′36.36″	–0.3445	0.4810	0.4672	0.1874
	21°34′22.95″	88°17′42.24″	–0.3299	0.4937	0.4097	0.2549
Pisciculture	21°34′10.37″	88°17′7.19″	0.1845	0.6850	0.4484	0.0580
	21°34′32.76″	88°17′34.77″	0.2547	0.5910	0.4862	0.1107
	21°34′47.65″	88°17′23.60″	0.2282	0.6219	0.4304	0.0683
	21°34′37.24″	88°17′33.51″	0.1456	0.7507	0.4193	0.0225
	21°34′46.46″	88°17′40.19″	0.1946	0.6683	0.4143	0.0800
	21°34′56.91″	88°17′34.38″	–0.2438	0.6058	0.4277	0.0351
	21°34′55.78″	88°17′33.15″	–0.2202	0.6347	0.4680	0.0832
	21°34′32.28″	88°17′33.55″	–0.1427	0.7583	0.4575	0.1063
	21°34′30.60″	88°17′31.10″	–0.1668	0.7176	0.4709	0.1116
	21°34′52.34″	88°17′26.43″	–0.1967	0.6657	0.4391	0.0624
Agriculture	21°34′59.76″	88°16′30.25″	–0.2677	0.5950	0.9040	0
	21°34′47.18″	88°16′49.61″	–0.2478	0.6160	0.7782	0
	21°34′12.61″	88°16′51.40″	–0.0066	0.9794	0.8857	0
	21°34′44.51″	88°16′57.85″	–0.2487	0.6210	0.8302	0
	21°34′59.28″	88°16′30.25″	–0.2652	0.5951	0.8832	0
	21°34′44.64″	88°16′30.47″	–0.3043	0.5442	0.9295	0
	21°34′4.18″	88°16′58.45″	–0.3925	0.4227	0.8465	0
	21°34′19.47″	88°16′46.14″	0.0805	1.1630	1.0134	0
	21°34′36.61″	88°16′59.96″	–0.2912	0.5553	0.8702	0
	21°34′20.37″	88°16′45.99″	0.1033	1.2189	0.9640	0
Beach	21°35′16.01″	88°17′56.45″	–0.2284	0.6528	0.9136	0
	21°35′22.34″	88°17′47.81″	–0.1694	0.7349	0.9011	0
	21°35′11.82″	88°18′1.19″	–0.2785	0.5828	0.8168	0
	21°35′26.12″	88°17′41.94″	–0.2089	0.6762	0.9056	0
	21°35′19.54″	88°17′51.79″	–0.2093	0.6772	0.9365	0
	21°35′18.39″	88°17′53.08″	–0.2030	0.6845	0.9122	0
	21°35′26.29″	88°17′41.33″	–0.2089	0.6762	0.9056	0
	21°35′13.88″	88°17′58.26″	–0.2828	0.5803	0.9104	0
	21°35′15.44″	88°17′56.36″	–0.2594	0.6055	0.8855	0
	21°35′19.62″	88°17′52.31″	–0.1862	0.7113	0.9321	0
Mangrove forest	21°34′56.19″	88°17′54.45″	–0.2948	0.5445	0.4453	0.1446
	21°34′52.16″	88°17′50.07″	–0.2742	0.5696	0.4134	0.1623
	21°34′52.57″	88°17′49.46″	–0.2143	0.6470	0.4419	0.1496
	21°34′52.58″	88°17′47.48″	–0.2740	0.5697	0.4504	0.1568
	21°34′45.72″	88°17′51.75″	–0.3345	0.4986	0.4215	0.1979
	21°34′11.52″	88°17′38.41″	–0.2819	0.5601	0.4573	0.1771
	21°34′54.57″	88°17′52.96″	–0.2591	0.5883	0.4388	0.1595
	21°35′12.33″	88°17′48.33″	–0.3364	0.4964	0.4717	0.1720
	21°5′6.12″	88°18′2.97″	–0.4287	0.3998	0.4639	0.1731
	21°34′54.10″	88°17′51.56″	–0.3012	0.5370	0.4361	0.1577

minerals stored in the Jet Propulsion Laboratory (JPL) at USGS and identified accordingly.

The conventional salinity indices have been applied on the hyperspectral image data of the study area. The index values of saline blank soil, pisciculture soil and soil of dense mangrove forests have been estimated and analysed. The results have been compared with the output of the proposed SBDI, which shows that SBDI gives more

Table 4. Overall accuracy of salinity indices

Index	Classified pixels	Unclassified pixels	Overall accuracy
Salinity index	620/41402	40782/41402	1.49
Normalized differential salinity index	304/41402	41098/41402	0.73
Saline blank detection index	30606/41402	10796/41402	73.92

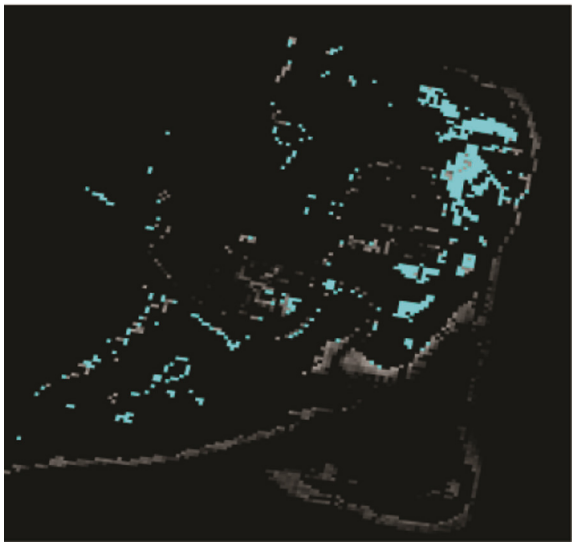

Figure 6. Saline soil (cyan) after saline blank index application.

Figure 7. Saline areas identified with NDSI.

accurate results for saline blank areas compared to other indices (Table 3). As shown in Table 3, the NDSI values are mostly negative. It is observed that SI values of saline blanks are in the range 0.6–0.7, whereas those of pisciculture show higher index values although they have lower salinity than saline blanks. As our objective is to identify saline blank areas with very high salinity, they could be accurately detected with the proposed index. Application of the index extracts saline blank pixels specifically observed to have index values above 0.1. The saline soil pixels from dense mangrove forests have lower SBDI values than saline blank pixels indicating lesser salinity, while the pisciculture soil shows lower SBDI values than soil pixels from dense mangrove forests. Thus SBDI gives a more accurate output compared to SI.

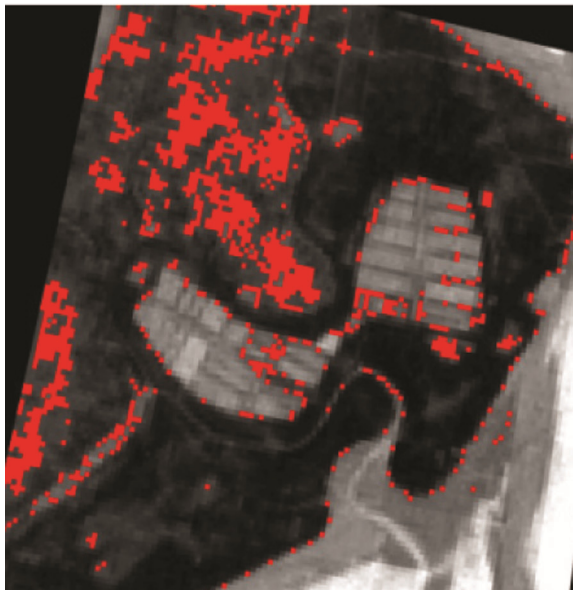

Figure 8. Saline areas identified with SI.

Figures 7 and 8 indicate the identified areas of saline soil after application of NDSI, SI and SBDI on the hyperspectral image of the study area.

For justifying the accuracy of the new index, its values have been compared with the existing indices (Table 4). Overall accuracy is the ratio of total number of correctly classified pixels to total number of pixels in the image. When SI and NDSI were applied, they have identified all saline soils in the study area apart from saline blank pixels. It is observed that SBDI successfully identifies only saline blank pixels in the study area (which is our objective), whereas the indices identify all types of saline soils. Thus, in this case, the total number of pixels misclassified as saline blank pixels is very high, and leads to very low accuracy values for SI and NDSI when compared with SBDI. Saline blanks occupy a small percentage of the total saline soil pixel area of the Henry

Island; so the number of misclassified pixels is also very high leading to 1.49% accuracy for SI and 0.73% accuracy for NDSI. The proposed index has identified saline blank pixels with an accuracy of 73.92%. The salinity of pixels representing different types of saline soils has also been physically tested and analysed, and then compared with the SBDI values for assessment of accuracy (Table 3).

It may be concluded after ground validation that SBDI detects saline blanks most accurately compared to the other indices.

In this study we have developed an index on hyperspectral image data for automatic detection of saline blanks amidst dense mangrove forests of the Sunderban Biosphere Reserve. We have successfully detected the hyperspectral bands that indicate the presence of minerals present in saline blank areas. The developed index has been compared with existing salinity indices (NDSI and SI). It is found that the former performs better than the latter, and accurately detects the saline blank areas of Henry Island of the Sunderbans Delta.

1. Schmid, T., Koch, M. and Gumuzzio, J., Applications of Hyperspectral. *Remote Sensing of Soil Salinization: Impact on Land Manage.*, 2008, p. 113.
2. Barik, J. and Chowdhury, S., True mangrove species of Sundarbans delta, West Bengal, eastern India. *Check List*, 2014, **10**(2), 329–334.
3. Samanta, K. and Hazra, S., Landuse/landcover change study of Jharkhali Island, Sundarbans, West Bengal using remote sensing and GIS. *Int. J. Geomatics Geosci.*, 2012, **3**(2), 299.
4. Ghosh, M. K., Kumar, L. and Roy, C., Mapping long-term changes in mangrove species composition and distribution in the Sundarbans. *Forests*, 2016, **7**(12), 305.
5. Nayak, S. and Bahuguna, A., Application of remote sensing data to monitor mangroves and other coastal vegetation of India. *Indian J. Geo-Mar. Sci.*, 2001, **30**(4), 195–213.
6. Hazra, S., Ghosh, T., Das Gupta, R. and Sen, G., Sea level and associated changes in the Sundarbans. *Sci. Cult.*, 2002, **68**(9/12), 309–321.
7. Hazra, S. and Samanta, K., Temporal Change Detection (2001–2008): Study of Sundarban, 2016, No. id: 10526.
8. Danda, A. A., Sriskanthan, G., Ghosh, A., Bandyopadhyay, J. and Hazra, S., Indian Sundarbans delta: a vision. World Wide Fund for Nature, New Delhi, 2011.
9. Mukhopadhyay, A., Dasgupta, R., Hazra, S. and Mitra, D., Coastal hazards and vulnerability: a review. *Int. J. Geol., Earth Environ. Sci.*, 2012, **2**(1), 57–69.
10. Dehaan, R. and Taylor, G. R., Image-derived spectral endmembers as indicators of salinisation. *Int. J. Remote Sensing*, 2003, **24**(4), 775–794.
11. Singh, R. P. and Sirohi, A., Spectral reflectance properties of different types of soil surfaces. *ISPRS J. Photogramm. Remote Sensing*, 1994, **49**(4), 34–40; http://dx.doi.org/10.1016/0924-2716(94)90045-0.
12. Fernandez-Buces, N., Siebe, C., Cram, S. and Palacio, J. L., Mapping soil salinity using a combined spectral response index for bare soil and vegetation: a case study in the former Lake Texcoco, Mexico. *J. Arid Environ.*, 2006, **65**(4), 644–667.
13. Ben-Dor, E., Patkin, K., Banin, A. and Karnieli, A., Mapping of several soil properties using DAIS-7915 hyperspectral scanner data – a case study over clayey soils in Israel. *Int. J. Remote Sensing*, 2002, **23**(6), 1043–1062.
14. An, D., Gengxing, Z., Chunyan, C., Zhuoran, W., Ping, L., Tongrui, Z. and Jichao, J., Hyperspectral field estimation and remote-sensing inversion of salt content in coastal saline soils of the Yellow River Delta. *Int. J. Remote Sensing*, 2016, **37**(2), 455–470.
15. Baldridge, A. M., Hook, S. J., Grove, C. I. and Rivera, G., The ASTER Spectral Library Version 2.0. *Remote Sensing Environ.*, 2009, **113**(4), 711–715.
16. Narmada, K., Gobinath, K. and Bhaskaran, G., Monitoring and evaluation of soil salinity in terms of spectral response using geoinformatics in cuddalore environs. *Int. J. Geomat. Geosci.*, 2002, **5**(4), 536.
17. Allbed, A. and Lalit Kumar, Soil salinity mapping and monitoring in arid and semi-arid regions using remote sensing technology: a review. *Adv. Remote Sensing*, 2013, **2**(4), 373.
18. Ondrasek, G., Zed, R. and Szilvia, V., Soil salinisation and salt stress in crop production. In *Abiotic Stress in Plants – Mechanisms and Adaptations*, 2011.

Received 8 January 2018; revised accepted 26 March 2018

doi: 10.18520/cs/v115/i3/541-548

Contrasting observation in culturable aerobic and micro-aerophilic heterotrophic fish gut-bacteria: intestine-breathing *Lepidocephalichthys guntea* (Hamilton Buchannan) versus gill-breathing *Labeo rohita*

Rudra Prasad Roy[1], Tilak Saha[1,2] and Ranadhir Chakraborty[1,*]

[1]Omics Laboratory, Department of Biotechnology, and
[2]Immunology Laboratory, Department of Zoology,
University of North Bengal, Siliguri 734 013, India

Lepidocephalichthys guntea **exhibits exceptional adaptive characters and can survive in flowing or stagnant waters as well as muddy hypercarbic condition resembling a desiccating habitat. This study was conducted to relate aerophilic (both aerobic and micro-aerophilic) bacterial density in the gut of** ***L. guntea*** **with dissolved oxygen (DO_2) content. Aerophilic bacterial density in the gut of** ***L. guntea*** **was found independent of DO_2 content, as the air pocket(s) present in the gut balances the deficit of oxygen obtained through gill respiration. This phenomenon was found to be reversed in gill-breathing fish like** ***Labeo rohita*** **because the additional mechanism to breathe air via gut is absent. The density of both the categories of**

*For correspondence. (e-mail: rcnbusiliguri@gmail.com)